Science of the Total Environment 921 (2024) 171274

Contents lists available at ScienceDirect

Science of the Total Environment

journal homepage: www.elsevier.com/locate/scitotenv

Far-field effects of the Nile damming on the silica cycle in the Southeastern Mediterranean Sea

Timor Katz [a,*], Revital Bookman [b], Barak Herut [a,b,1], Beverly Goodman-Tchernov [b], Guy Sisma-Ventura [a,1]

[a] Israel Oceanographic & Limnological Research, National Institute of Oceanography, Haifa, Israel
[b] University of Haifa, Dr. Moses Strauss Department of Marine Geosciences, Leon H. Charney School of Marine Sciences, Haifa, Israel

HIGHLIGHTS

- First far-field study on damming effects on the silica cycle in an oligotrophic sea
- Nile damming stopped autumn floods terminating *DSi* seasonality in the sea.
- The damming greatly reduced *BSi* accumulation rates in deep-sea sediments.
- Mesoscale transport affected BSi accumulation >400 km from the Nile.

GRAPHICAL ABSTRACT

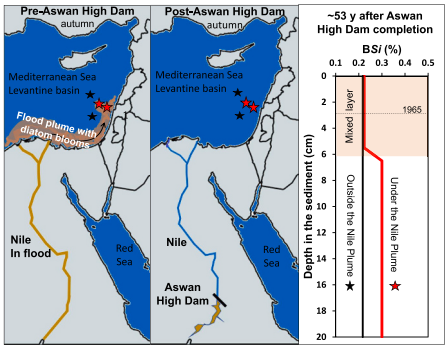

ARTICLE INFO

Editor: Olga Pantos

Keywords:
Levantine Basin
Nile
Damming
Biogenic silica
Sediments
Mediterranean Sea

ABSTRACT

Silica plays a key role in the growth of silicifying primary producers (e.g., diatoms) and hence the ocean carbon pump. The Mediterranean Sea's eastern Levantine Basin (ELB) is a low silica (and low N and P) ultra-oligotrophic basin. Before 1965, Nile autumn floods were a major source of dissolved silica (*DSi*) and other nutrients to primary producers of the ELB continental shelf, also known as the Nilotic cell. The construction of the Aswan High Dam (AHD) in the mid-1960s, blocked these floods, drastically diminishing the autumn-diatom blooms offshore the Nile delta. However, the far-reaching and long-lasting effects of the Nile damming on the Si cycle in the ELB remain unclear. Here, we studied the changes in *DSi* in the surface water offshore Israel and the distribution of biogenic silica in deep-sea short sediment cores, collected hundreds of kilometers from the Nile outlet, at depths range of 1100–1900 m, offshore the ELB Israeli coast. We show post dam reduction and termination in flood related seasonality of *DSi* and a concurrent decrease (of up to 79 %) in biogenic silica (*BSi*) accumulation rates in surficial sediments relative to underlying sediments. These changes reflect the effects of Si (dissolved and particulate) retention by the AHD on diatoms production, export and burial in the ELB. This far-field effect was demonstrated in deep-sea areas subjected to intense lateral transport of resuspended sediments from the shelf via intermediate nepheloid layers and to coastal water intrusions, along the path of the pre-dam,

* Corresponding author.
E-mail address: timor@ocean.org.il (T. Katz).
[1] Equal contribution.

https://doi.org/10.1016/j.scitotenv.2024.171274
Received 14 November 2023; Received in revised form 14 February 2024; Accepted 23 February 2024
Available online 24 February 2024

flood plumes. Our core records show that the AHD worsened nutrient-diminished, exceptionally unfavorable conditions for diatoms that persisted in the deep ELB at least during the last four millennia.

1. Introduction

Silicon is a key nutrient in the ocean, required for the growth of a large group of primary producers of silicifying organisms, including diatoms, radiolarians, silicoflagellates, and some sponges and choanoflagellates (Tréguer and De La Rocha, 2013). Diatoms, which require silica for the construction of their skeletons, are dominant primary producers responsible for up to 45 % of the organic carbon production in the ocean (Yool and Tyrrell, 2003). The biogeochemical cycle of silica in the ocean is, therefore, strongly intertwined with the biological carbon pump, affecting the inventory of carbon dioxide in the atmosphere (Wollast, 1974; Tréguer et al., 1995; Smetacek, 1999; Pondaven et al., 2000; Ragueneau et al., 2006; Laruelle et al., 2009). Nonetheless, the relative importance of diatoms in the phytoplankton community may vary, depending on nutrient stoichiometry and dissolved silica (D*Si*) availability in the water column (Leynaert et al., 2001, 2004), their contribution diminishing in nutrient and silica-depleted water compared to replete areas (Kamykowski et al., 2002).

Dissolved silica, originating from weathering of continental rocks is discharged into the coastal zone by rivers and groundwater (e.g. Bernard et al., 2010, 2011; Conley, 1997). Rivers also transport significant quantities of particulate amorphous silica that may later dissolve in the sea. Similarly, dust deposited may dissolve on the ocean's surface delivering silica to the photic zone (Tréguer and De La Rocha, 2013). Human activity during the 20th century altered river loads (both entrained sediments and solutes) that reach the oceans, mainly by construction of water reservoirs for electricity production and irrigation (Humborg et al., 1997; Ittekkot et al., 2000; Papush and Danielsson, 2006; Ludwig et al., 2009). The damming of rivers, stimulates the growth of diatoms and the retention of Si in reservoirs, resulting in a decrease in the riverine loads of DSi (Humborg et al., 1997; Conley et al., 2000). This phenomenon has been observed as a decrease in DSi concentrations in rivers and estuaries (Ittekkot et al., 2000; Laruelle et al., 2009; Bernard et al., 2011), draining into coastal water (Humborg et al., 1997, 2006, 2008; Papush and Danielsson, 2006). For example, in Finnish and Swedish rivers DSi have decreased in relation to the number of reservoirs in the catchment area (Humborg et al., 1997; Conley et al., 2000). The damming of the Danube River, which formerly contributed inputs of fresh water into the Black Sea, resulted in massive retention of silica since a dam was built in 1970–72 (Humborg et al., 1997).

Analogies can be drawn between the effects of damming the Danube on the Black Sea and that of the Nile damming on the East Mediterranean Sea (Milliman, 1997; Turley, 1999). Similarly, the Aswan High Dam (AHD) holds back massive amounts of silica carried by the Nile from entering the eastern Mediterranean Sea (Turley, 1999; Nixon, 2003; Chen et al., 2021). Dissolved silicate concentrations at the mouth of the Nile dropped by almost 200 μmol L^{-1} after the AHD began operation (Whaby and Bishara, 1980). Prior to the construction of the AHD, the annual Nile flood delivered about 7–11 × 10^3 t of biologically available phosphorus (P), at least 7 × 10^3 t of inorganic nitrogen (N), and 110 × 10^3 t of silica (*Si*) to the Mediterranean coastal waters off Egypt and Israel (Nixon, 2003). These nutrients stimulated a dramatic bloom of diatoms which supported a productive fishery (Halim, 1960). After the closure of the dam in 1965, the annual Nile floods and related nutrients (N, P, Si) discharge dropped by ~90 % and the blooms offshore the Nile delta disappeared causing fishery collapse (Nixon, 2003; Dowidar, 1984). The DSi discharge from the Nile remained low thereafter whereas N and P retention behind the dam was gradually compensated by enhanced inputs of sewage and fertilizers down river (Nixon, 2003). Pre-AHD, observations note that after the floods, a plume of relatively turbid, low salinity, nutrient-rich water from the Nile used to gradually flow from the discharge area, along the coast of Egypt, Israel, and ultimately Lebanon (Emery and Neev, 1960). Consequently, the damming of the Nile has influenced the productivity, biogeochemistry and food web structure in the Eastern Mediterranean Sea (Bialik and Sisma-Ventura, 2016; Turley, 1999), in particular along its southeastern shelf (Halim, 1960, 1991; Herut et al., 2023).

This massive ongoing reduction in DSi owing to changes in the Nile discharge after the construction of the AHD had apparent proximate effects offshore the Nile delta (Nixon, 2003; Chen et al., 2021). However, the long-term and far-field effects of the AHD on the silica cycle and diatoms abundance in the Mediterranean Sea's eastern Levantine Basin (ELB) remain unknown. Bridging this knowledge gap has implications for damming effects on the marine silica cycle in the ocean in general. It is however of particular interest considering that damming effects on the Si cycle were mostly investigated in nutrient and DSi replete marine regions e.g. the Baltic and Black seas (Humborg et al., 1997, 2006, 2008; Papush and Danielsson, 2006) while very little is known about them in oligotrophic seas such as the ELB. In this study, we used historical, long-term, water column D*Si* data and deep-sea (1100–1900 m) short sediment cores (beyond the continental slope of the ELB offshore Israel), hundreds of kilometers from the Nile Delta, to study if and how the construction of the AHD affected the opal accumulation rates. These observations enabled exploring the long-term and far-field effects of the AHD on the silica cycle in the ELB.

2. Materials and methods

2.1. Study area

This study was conducted in the ELB, offshore Israel (Fig. 1), which owing to the Mediterranean Sea general anti-estuarine circulation (Pinardi and Masetti, 2000) and relatively low nutrient inputs (Krom et al., 2004) is one of the most oligotrophic provinces worldwide (Reich et al., 2022). The continental margins of the ELB are typified by warm (>17–31 °C) and well-oxygenated surface water, with extremely low, both, PO_4 and $NO_3 + NO_2$ levels (typically <20 and 80 nM respectively; Fig. 2), and primary production rates (~32 g C m^{-2} y^{-1}) (Rahav et al., 2019; Reich et al., 2022). It is also considered as a low DSi marine province, typically averaging ~1.0 μM (Herut et al., 2000; Kress and Herut, 2001; Kress et al., 2014; Krom et al., 2014). These unique water characteristics are driven by climate and anthropogenic processes, and have the potential for global significance in understanding the silica cycle in oligotrophic oceanic basins more generally.

2.2. Fieldwork

2.2.1. Sediment sampling

Sampling campaigns of deep-sea sediments were conducted by the R. V. Bat Galim during 2017–2018, performed by the Israel Oceanographic and Limnological Research (IOLR) as part of the National Monitoring Program of Israel's Mediterranean waters (Table 1). Sediments cores were retrieved with a box-corer (Ocean Instrument 650 BX) using Perspex push corers (i.d.: 5 cm) and cut into vertical sections of 0.5–1.0 cm. The first few cm's were sliced at high resolution (5.0 mm) and the subsamples were kept refrigerated and/or frozen for laboratory processing.

Four short (20–25 cm) sediment cores were chosen for down-core analysis of their chemical and elemental properties (Table 1), based on their location with respect to the mesoscale circulation features driven by surface currents. Cores H04 and H05 are located within the path of coastal-open-sea intrusion features off the Carmel submerged

ridge (Efrati et al., 2013; exemplified by the westwards Chlorophyll-a plume in Fig. 1), while TA05 and G05 were collected from peripheral, open sea areas. As an extension of the long-shore currents (Inman, 2003; Malanotte-Rizzoli et al., 2014; Fig. 1), these mesoscale intrusions from the shelf may deliver nutrients and terrigenous material from the Nile Delta and continental shelf (Azov, 1991; Efrati et al., 2013; Herut et al., 2023), resulting with the formation of dynamically isolated niches in the ultra-oligotrophic ELB. In addition, stations H04 and H05 are located at a lateral sediment transport corridor from the northern Israeli continental shelf and slope by nepheloid layers (Katz et al., 2020) and by turbidity currents along slope-confined submarine canyon (Jaijel et al., 2023).

2.2.2. Water sampling

Depth-profiles of nutrient concentrations at the stations in Table 1 during 2002–2022 were conducted as part of the National Monitoring Program of Israel's Mediterranean waters, focusing on $NO_2 + NO_3$ (NO_x), PO_4, and $Si(OH)_4$ (D*Si*) (Fig. 2), which are the main limiting nutrients in the photic zone affecting diatom growth. Seawater samples were collected using a Niskin bottles Rosette sampler (carousel with SeaBird profiler SBE911plus) for dissolved inorganic nutrients analysis. In addition, we analyzed D*Si* time series of the surface layer in Israeli continental shelf to elucidate long-term trends (Fig. 3). The open water D*Si* data spanned the period between 1963 and 2022, including the pre-AHD final damming period in 1965. Data of D*Si* concertation of the deep-sea stations were compiled for the period of vertical mixing (between December and June) and the period of stratification (between July and December), also including the flooding season between August and December. The raw data between 1963 and 2002 was obtained from the ISRAMAR data center: https://isramar.ocean.org.il/isramar2009. We also analyzed DSi surface water data from the shelf (stations between 10 and 125 m water depth) sampled in 1964 (ISRAMAR data center), capturing a significant Nile flood event, last to reach offshore Israel prior to the final operation of the AHD in 1965 (Halim et al., 1967). To the best of our knowledge, these historical measurements are the only record of DSi concentrations of a Nilotic flood on the ELB water column (Fig. 3).

2.3. Laboratory analyses

2.3.1. Biogenic silica (BSi) analysis

The analysis of the biogenic silica content in sediment samples followed the methodology of Conley and Schelske (2001) with slight modifications. Briefly, frozen sediments were lyophilized for 48 h and

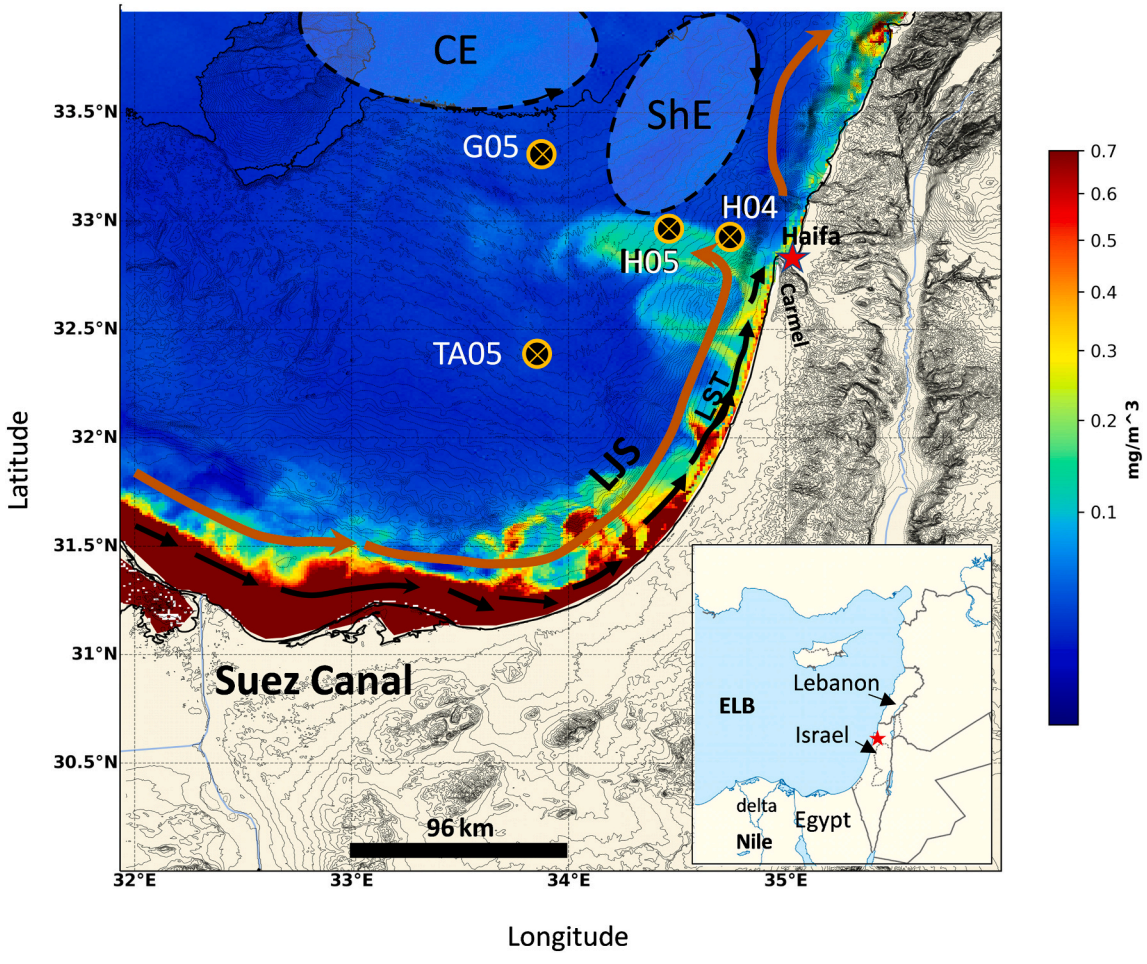

Fig. 1. Map of the study area, showing the continental margins of the ELB at the Southeastern Mediterranean Sea. Typical distribution of chlorophyll-a (Chl-*a*) from satellite imaging (data from https://isramar.ocean.org.il/isramar2009/) is shown stretching across the Nile littoral cell (Inman and Jenkins, 1984), from the Nile Delta in the southeast along the coast of Sinai, Egypt, proceeding on a northward track along the Israeli coast. Note the plume of Chl-*a* accompanying a coastal water intrusion offshore Haifa (Efrati et al., 2013). Also presented on the map are the city of Haifa (red star), the Carmel ridge and the sampled sediment core locations (crossed circles) and the schematic hydrological current system and gyres of the Southern ELB, after Malanotte-Rizzoli et al. (2014): The Levantine Jet System (LJS, also known as Libyo-Egyptian current) and the sub-mesoscale Cyrprus and Shikmona Eddies (CE and ShE). The Longshore Sediment Transport (LST) is denoted by black arrows after Inman (2003). A regional map of the east Levantine basin of the Mediterranean Sea, including the Nile Delta is inset at the top-left of the figure. (NordNordWest – Own work using: World Data Base II data, CC BY-SA 3.0 de, https://commons.wikimedia.org/w/index.php?curid=25432681).

then sieved through a 1000 μm sieve to remove the larger fraction. Samples were not mill ground to ovoid exposure of new surfaces for dissolution. No significant differences in B*Si* concentration has been found for sample weights between 20 and 40 mg of dry sediments. We used a consistent weight of 40 mg for all samples because of the expected low concentrations of B*Si* in deep-sea, ELB sediments. Weighed, freeze-dried sediments were placed into 50 ml polypropylene *DigiTubes* (SCP Science). The alkaline digestion was initiated by addition of 40 ml 1 % Na_2CO_3 and placing the tubes in covered shaking bath at 85 °C and 100 rpm with caps slightly loosened to vent gases. At three time points, after 3, 4, and 5 h of digestion, the tubes were removed, placed into an ice bath and cooled for 5 min to stop further dissolution. At each time point the tubes were sub-sampled (1 ml) into 9 ml of 0.021 N HCl acid to neutralize the solution. The BSi content in the sample was calculated from the intercept of the regression line of the DSi concentrations with the y axis in the three time points. The excellent regression coefficient ($r^2 > 0.994$) validates the sensitivity and adequacy of the extraction methodology for measuring sedimentary low B*Si* levels. Two reputability trials, each conducted with five sediment subsamples yielded RSD of 10.5 %. The weight fraction of biogenic silica in the sediment samples (f_{BSi}) was calculated in the following manner:

$f_{BSi} = ([DSi_{ic}] \times V \times M_{Si}) / W_s$ where: $[DSi_{ic}]$ is the dissolved silica concentration at the intercept between the regression line and the y axis, V is the volume in the test tube, M_{Si} is the molar mass of Si and W_s is the weight of the sediment sample. The opal fraction in the sediment was calculated by multiplying f_{BSi} by 2.4 (Mortlock and Froelich, 1989).

The D*Si* (silicic acid) concentration was determined using a segmented flow Seal Analytical AA3 using the reaction with ammonium molybdate in an acidic medium to form silicomolybdic acid, which is reduced to the molybdenum blue with stannous chloride and the absorption is measured at 820 nm. The reproducibility of the analyses was determined using certified reference materials (CRM): MOOS 3 and VKI 4.2. Results were accepted when measured CRM's were within ±5 % from the certified values. The reproducibility of the wet alkaline extraction was determined by analyzing replicates of sediments from the study site (±0.015 %) and blanks. For the calibration curve, we used a stranded D*Si* ($Si(OH)_4$) solution at a concentration of 10 mM in a DDW medium. The range of calibration was set at 50 μM, where the measured values of the extractions were typically between 10 and 40 μM.

Dissolved inorganic nitrate+nitrite ($NO_3 + NO_2$) and orthophosphate (PO_4) were determined using a Seal auto-analyzer system with colorimetric detection. Quality control of the nutrient results along the years was performed with the use of internal and certified reference standards and by the participation in international laboratory performance exercises (QUASIMEME; Sisma-Ventura et al., 2021).

^{210}Pb activity was determined from the activity of its granddaughter isotope ^{210}Po, assuming secular equilibrium and correcting the elapsed time since the samples' collection (Noller, 2000). The dry samples were homogenized and sieved through a 63 μm plastic sieve to reduce the particle-size related variation of ^{210}Po and to increases activity detection. Approximately 0.5 g of the sediment was spiked with 1 ml of a standard solution of ^{209}Po in 2MHCl, and then leached for 6 h in 10 ml of concentrated hydrochloric acid heated to 95 °C to extract ^{210}Po from the sediment. After diluting the fluid with 45 ml of demineralized water and adding 5 ml of an aqueous solution of ascorbic acid (40 g l^{-1}), the natural ^{210}Po and the added ^{209}Po were collected from the fluid by spontaneous electrochemical deposition on silver plates, which were suspended in the heated fluid (80 °C) for at least 16 h. The Po isotopes collected on the silver plates were then measured by Octete Plus alpha-spectrometer using Implanted Planar Silicon detectors, with a count time of 3 days, which is sufficient to reduce the counting error to be 3 %.

Table 1
Sediment cores sampling locations and analyses. Analyzed variables are coded in the following manner: porosity (por), biogenic silica (BSi), particulate organic carbon (POC), ^{210}Pb, major elements (MEl), grain size distribution (GSD). BSi in all of the cores and MEl in H04 were measured at high (0.5–1 cm) resolution from the surface to the bottom.

Station ID	Lat °N	Long °E	Water Depth (m)	Analyzed variables
TA05	32.42481	33.77777	1400	por, BSi, POC, ^{210}Pb, MEl
H04	32.95017	34.75100	1100	por, BSi, POC, ^{210}Pb, MEl, GSD
H05	32.99950	34.50100	1450	por, BSi, POC, ^{210}Pb, MEl
G05	33.34933	33.92167	1950	por, BSi, POC, ^{210}Pb, MEl

2.3.2. Organic carbon (OC)

OC content in the sediment was determined by wet oxidation with potassium dichromate and sulfuric acid with the residual dichromate using the (slightly modified, potentiometric) titration method by Gaudette et al. (1974) with $(NH_4)_2Fe(SO_4)_2$.

2.3.3. Major elements (Si, Ca and Al)

Major elements in sediments were determined with an ED-XRF (SPECTRO-SCOUT). Two grams of oven dried, powdered sediment subsamples were analyzed in the machine vacuum chamber and the results were calibrated with readings from 5 to 7 certified sediment standards as described in Zirks et al. (2021).

2.3.4. Granulometry

Grain size distribution (as volume%) in the sediment was measured using the laser diffraction technique with a Malvern Masterseizer-3000. The readings were conducted following digestion of organic matter with H_2O_2, dispersion with Sodium Hexametaphosphate ('Calgon') and sonication as described in the marine sediments pretreatment protocol (PT4SD) by Jaijel et al. (2021).

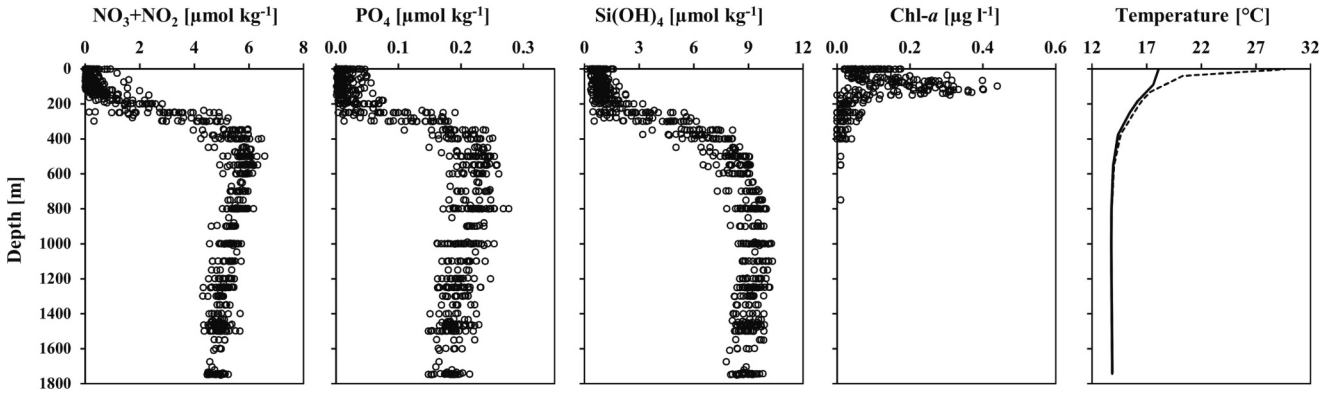

Fig. 2. Water column profiles of Nitrate+Nitrite ($NO_3 + NO_2$), Orthophosphate (PO_4), silicic acid (D*Si*), Chlorophyll-*a* during 2002–2022 and representative winter (solid line) and summer (dashed line) temperature down to ~1800 m depth.

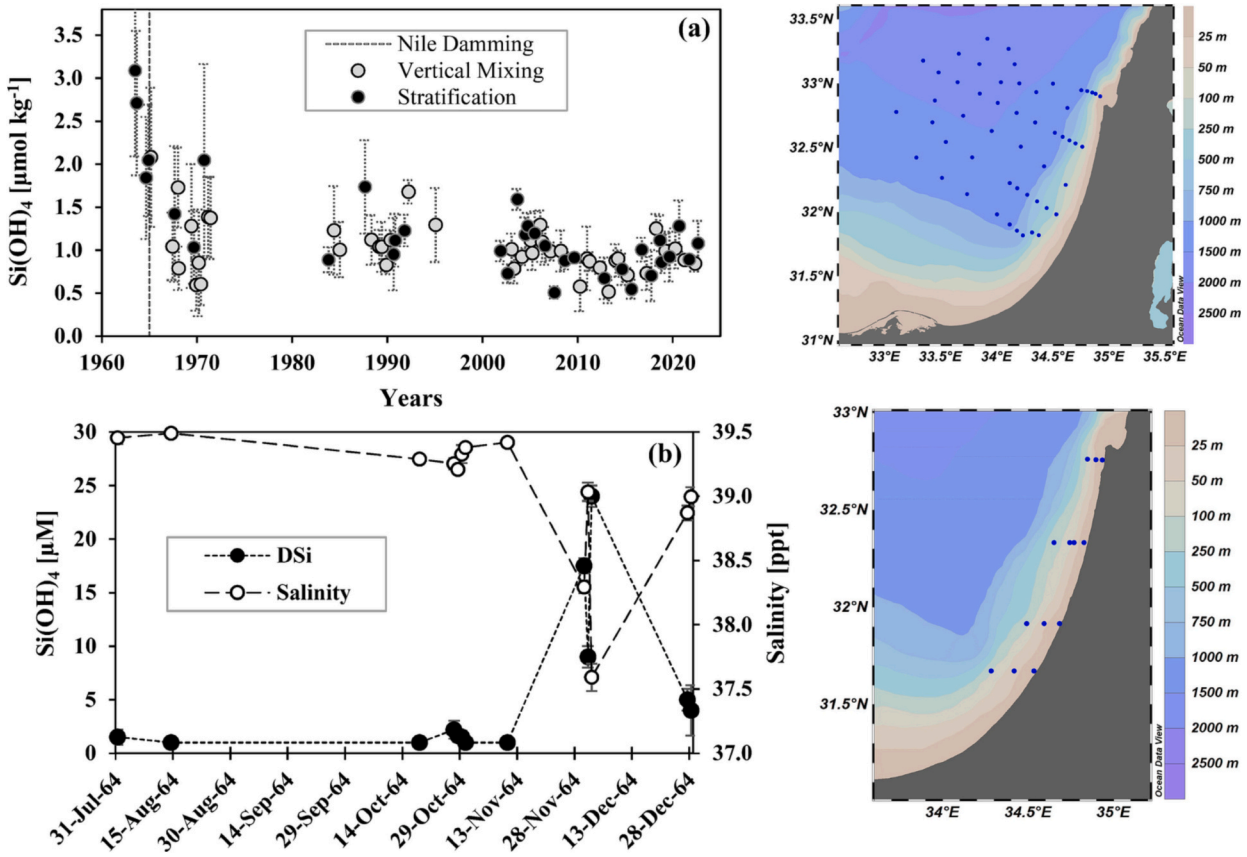

Fig. 3. Time series compilation of average (± SD) D*Si* ($Si(OH)_4$) concentrations in surface seawater: (a) in open water cruises (see map a1) and (b) Averaged over the continental shelf of Israel in 1964 (sampling points are presented on a bathymetric map b1), before during, and after the arrival of a massive flood plume from the Nile during an event, occurring in November and December 1964 (sampling dates in: 31.7; 14.8; 18.10; 27–30.10; 10.11; 30.11; 1–2.12; 20.12; 27–28.12). Sampling points during cruises are presented on a bathymetric maps a1 and b1. The open water data was averaged for each cruise, therefore, representing the mean DSi during cruises. The maps show the entire sampling points of DSi for the entire study period, yet not all stations were sampled in each cruise.

3. Results and discussion

3.1. Temporal changes of dissolved silica

Time series of DSi ($Si(OH)_4$) concentrations in surface waters of the Southeastern ELB shows somewhat higher pre-AHD concentrations for the period 1962–1965 during the season of stratification (coinciding with the past Nile flooding season), varying on average between 1.84 ± 0.71 and 3.09 ± 1.04 µmol kg^{-1} (Fig. 3a). No such differences were observed for the season of vertical mixing, averaging 1.17 ± 0.49 µmol kg^{-1} in 1962–1964, and 1.16 ± 0.27 µmol kg^{-1} for the period 1983–1995. Since 2002, the open surface water yielded an average D*Si* value of 0.85 ± 0.21 µmol kg^{-1} and variations in and between the years and seasons diminished (Fig. 3a). These results demonstrate that at present, D*Si* concentrations in the ELB surface water are amongst the lowest worldwide, between 0.4 and 1.6 µmole Kg^{-1}, with no clear seasonal trend in the last few decades (Herut et al., 2000; Kress and Herut, 2001; Figs. 2 and 3). Furthermore, they are more akin to mid-oceanic, oligotrophic gyres e.g. the North Pacific subtropical gyre, where D*Si* concentrations generally range between 0.8 and 1.25 µM (Brzezinski et al., 2011). Moreover, integrated D*Si* stocks of the upper 80 m in the northeast Atlantic (40–43.5 N, 15–21 W) were 40–57 mmol m^2 in late summer and between ~100 and 200 mmol m^2 in the winter (Leblanc et al., 2005). This is compared to 26–96 mmol m^2 in both summer and winter in the ELB in the last two decades (Fig. 2), similar to levels observed by Herut et al. (2000) considering the upper 80 m solely. These low DSi concentrations result from the anti–estuarine circulation of surface water, limited vertical mixing, and extremely low discharge of nutrients to the ELB from runoff and rivers (Kress et al., 2014; Krom et al., 2014). As with D*Si*, PO_4 and NO_X are also highly depleted in all seasons at the surface mixed layer of the ELB (Fig. 2), particularly during stratification in summer and autumn. During these periods, nutrient values are typically close to, or below the detection limit of the instruments in the surface/upper water column (9 nmol L^{-1} for PO_4, and 80 nmol L^{-1} for $NO_2 + NO_3$ (NO_x) (Fig. 2). This indicates a co-limitation of P, N, and Si for diatom growth in the ELB coastal water (Rahav et al., 2018). Below the photic layer, nutrient concentrations increased with depth to a maximum located between 400 and 800 m (Fig. 2). This allows for the delivery of D*Si* and other nutrients to the surface water during winter mixing (~200 m). Concurrently, diatom abundance in the ELB is now highest in winter and lowest in the stratified summer and autumn (Rahav and Berman-Frank, 2023). The ELB is recognized as a basin of severe nutrient limitation for primary production (Browning and Moore, 2023), amongst the lowest for any marine basin (~32 g C m^{-2} y^{-1}; Reich et al., 2022). Conditions are innately harsher for diatoms that are further limited by D*Si*.

Notably, the present conditions across the Israeli continental shelf are somewhat different than they were 5–6 decades ago. Pre-AHD (prior 1965), the surface water salinity was controlled by a balance between high rates of evaporation and ejected freshets from the Nile seasonal flooding. Decreasing salinities were observed seasonally up to the Lebanese shelf (Azov, 1991) maintained for several weeks following the Nile floods (Hecht, 1964; Bialik and Sisma-Ventura, 2016). This low salinity Nile floodwater contained high concentrations of DSi, as observed throughout the Israeli shelf after flood events (D*Si* concentrations increased up to 28.2 µmol kg^{-1}; Fig. 3b). This invers correlation between

salinity and DSi is exemplified in the only available set of measurements from offshore Israel collected soon after a Nile flood (Dec 1964; Fig. 3b). According to Halim (1960), the floods caused massive diatom blooms offshore the Nile delta. These events caused concurrent diatom blooms along the entire Nile plume trajectory (Oren and Komarovsky, 1960). However, following the completion of the AHD, floods were blocked and the DSi transport was reduced dramatically, remaining low thereafter (Nixon, 2003; Chen et al., 2021). Our data shows that this was in turn manifested in the overall reduction in DSi concentrations during the stratified period offshore Israel and the decrease in its seasonal variation, even in the open sea stations (Fig. 3a). The D*Si* variations recorded after 2000 may be attributed to the decadal reversals in the North Ionian Gyre, i.e. Bimodal Oscillation System (BiOS), as suggested by Ozer et al. (2017). As a result, while minor diatom blooms might still occur during winter and spring (Rahav and Berman-Frank, 2023), diatom concentrations during summer and autumn are minimal compared to the period prior to the AHD, when Nile floods used to trigger diatom blooms along the Southeastern coast of the ELB.

3.2. *Temporal and spatial changes in sedimentary biogenic silica and organic carbon*

The total particulate Si (lithogenic Si + B*Si*), Ca, and Al concentrations in the sediment cores at stations TA05, H04, H05, and G05 (Fig. 4) changed between sites but were fairly constant down the cores. The increase in Ca and decrease in Al concentrations between H04, H05, TA05, and G05 are attributed to the change in distances from the shelf-edge (Fig. 1). These differences are mainly attributed to the seaward decreasing fraction of lithogenic aluminosilicates derived from terrestrial sources with respect to calcareous plankton skeletons from marine sources (Katz et al., 2020). The B*Si* in these cores comprised approximately 1.3 % of the total Si in the sediment (Fig. 5) and is impacted by different factors as discussed below. The grain size distribution profile (not shown here) was analyzed only in the H04 sediment core showing also fairly stable median and mode values down core, ranging between 3 and 4 and 5 and 9 μm, respectively.

The sampling locations were designed to represent two types of deep-sea sedimentary areas: 1) impacted by lateral transport processes of both, coastal and pre-AHD flood-water and resuspended shelf sediments (stations H04 and H05; Fig. 1), and 2) deep-sea areas dominated by the general, basin-scale circulation and vertical particulate fluxes (stations G05 and TA05; Fig. 1). Thus, stations H04 and H05 are located *en-route* of the coastal, mesoscale water intrusion at the Rosh-Carmel (the submerged extension of the Carmel ridge; Efrati et al., 2013; Fig. 1) that following floods, innately, ejected Nile-plume water offshore. Moreover, these stations are greatly affected by the delivery of resuspended sediments from the shelf via intermediate nepheloid layers (Katz et al., 2020) and possibly by turbidity currents from submarine canyons to the north of the city of Atlit (Jaijel et al., 2023).

Fig. 5 show the BSi (equivalent to ~0.42 opal) and OC concentrations in the sediment cores collected from all the sites: TA05, H04, H05 and G05. The BSi concentrations varied between 0.16 and 0.37 % (0.4–0.9 % opal), which are amongst the lowest recorded in marine sediments, even compared to worldwide oligotrophic marine provinces (Dixit and Van Cappellen, 2003; Li et al., 2016; Xu et al., 2020; Sayles et al., 1996). This corresponds with both, very unfavorable conditions for diatoms growth i.e. exceptionally low DSi and nutrient concentrations in the photic layer and low preservation conditions of opaline skeletons. The latter being affected by the rapid dissolution owing to high degree of under-saturation and warm temperatures (>13.8 °C) at the ELB deep water (Fig. 2; Ragueneau et al., 2000; Van Cappellen and Qiu, 1997). Studies in Vermetidae-reef cores and sediments along the Israeli coastline revealed a rise in surface water temperature, stratification, and oligotrophication during the last ~150 years (Sisma-Ventura et al., 2014; Herut et al., 2023). This trend was notably aggravated in the ELB in recent decades (Ozer et al., 2017, 2022; Herut et al., 2023). Such conditions may further reduce diatoms growth and the dissolution of B*Si* in settling siliceous frustules, thereby, reducing B*Si* preservation (accumulation) in the sediment.

Significant changes were observed in the BSi distribution between the two types of sedimentary provinces. In the TA05 and G05 sediment cores, the mean BSi content averaged between 0.23 % (SD = 0.033 %) and 0.24 % (SD = 0.034 %), respectively, with no clear shifts down core. Contrarily, the BSi depth-profiles in the H04 and H05 sediment cores had significantly lower concentrations near the surface (upper ~5 cm) compared to further down core (*t*-Test: $P < 0.0001$), with inflection points at 5.5 and 5 cm depth, respectively (Fig. 5). The B*Si* content in the H04 core increases from a mean ± SD of 0.21 ± 0.03 % in the upper 5.5 cm to 0.34 ± 0.03 % further downwards and in H05 from 0.26 ± 0.03 % in the upper 5 cm to 0.3 ± 0.02 % downwards till the bottom of the core. This depth increasing shift is a unique observation since owing to fresh biogenic silica inputs, B*Si* depth-profiles are often higher near the surface relative to downcore (Ragueneau et al., 2001). It may therefore serve as an indication for an environmental change in these sampling areas. In addition, whereas above 6 cm depth, the B*Si* % in the peripheral TA05 and G05 cores was similar (~0.23 %) to H04 and H05 cores, below this depth, it was significantly ($P << 0.001$) lower (Fig. 5). Conversely, the OC depth profiles in all the sediment cores exhibited a normal depth decreasing trend ranging between 0.76 and 1.0 % near the surface to 0.3–0.65 % at 20 cm depth (Fig. 5).

The Si and C cycles in the ocean are linked by primary productivity of diatoms in the photic zone (Ragueneau et al., 2000), that in the ELB constitute a relatively small fraction of the primary producers (Krom et al., 2014; Rahav and Berman-Frank, 2023). However, the observations in the H04 and H05 sediment cores suggest that the process causing the near-surface deplete in B*Si* is di-coupled from the OC which increases

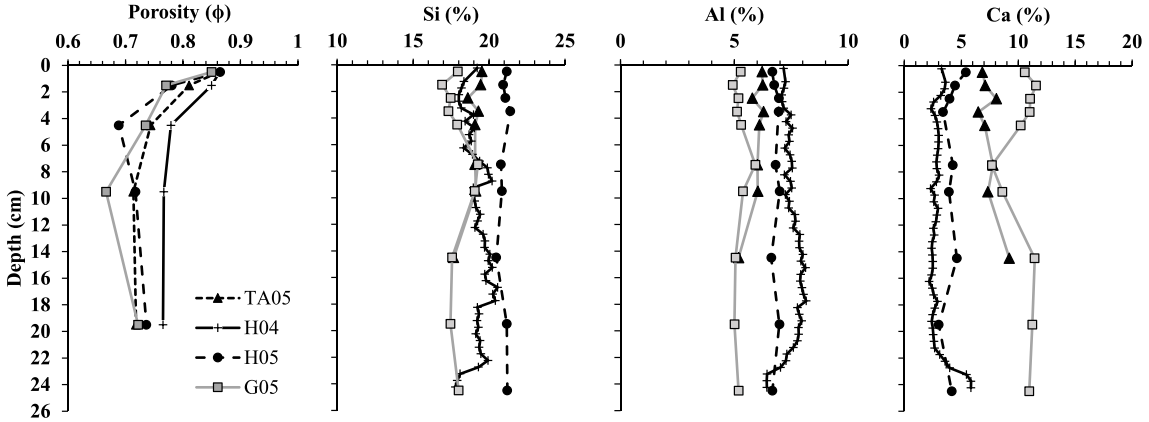

Fig. 4. Depth-profiles of porosity and of Si, Al and Ca concentrations (dry weight %) in the TA05, H04, H05 and G05 sediment cores.

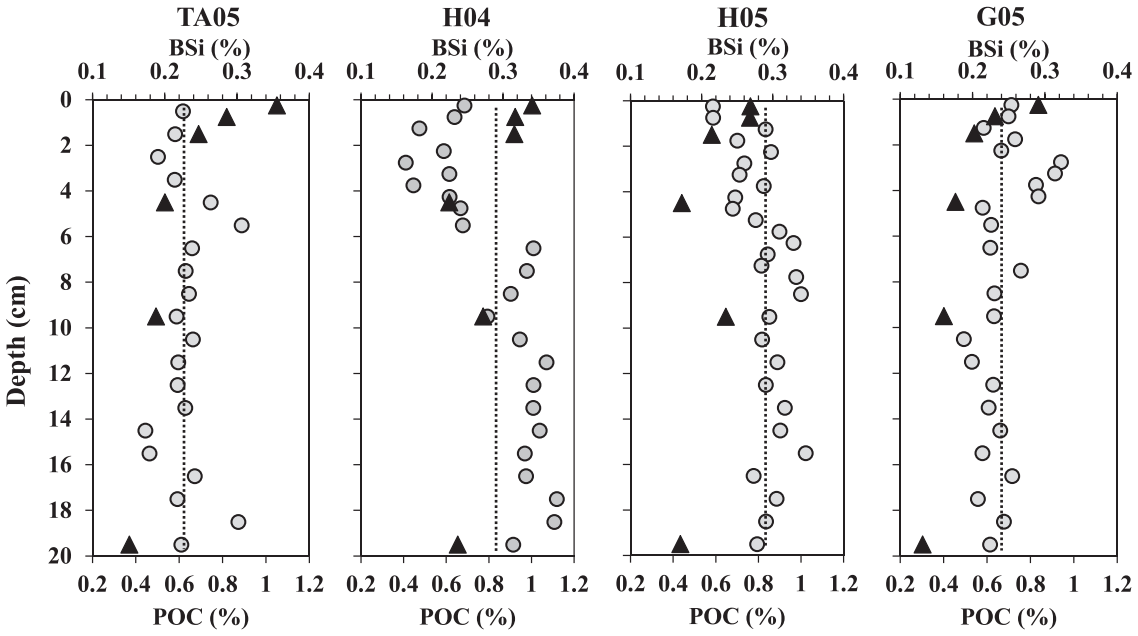

Fig. 5. B*Si* (0.42 opal; gray circles) and POC (black triangles) concentrations in sediment cores from sites TA05, H04, H05, and G05 (Fig. 1 and Table 1). The dashed line denotes the B*Si* mean concentration of all the samples in each of the cores.

towards the surface. Accordingly, the change in the accumulation of diatom skeletons (or BSi concentrations), solely in these stations depict an environmental shift while the organic carbon show normal behavior. This decoupling may be related to the fact that unlike D*Si*, much of the retained P and N behind the AHD were later compensated by downstream inputs of sewage and fertilizers (Nixon, 2003) such that diatoms were more affected than other primary producers. This assumption corresponds with somewhat higher total Ca concentrations near the surface in H04 and H05 (Fig. 4) noting also a decoupling (if not reversal) between calcifying photosynthesizing plankton such as foraminifers and silicifying diatoms. Additionally, it was recently suggested that C content in the sediments where B*Si* decreased (H04 and H05) is controlled by lateral transport from local streams (Alkalay et al., 2020) and therefore less affected by changes in the water column owing to the AHD.

The fact that the B*Si*% shift was only observed in two of the four cores (Fig. 5) precludes basin-wide warming and oligotrophication in the ELB as its main causes. We therefore propose that the observed decline in B*Si* towards the sediment surface in H04 and H05 is the result of the final damming of the Nile by the AHD since 1965. The AHD stopped the summer-autumn discharge of Nile floods to the ELB that used to deliver and elevate D*Si* concentrations (Fig. 3) trigger diatom blooms (Oren and Komarovsky, 1960), and supply fine sediments to and along the Israeli continental shelf (Herut et al., 2023). Following the Nile floods, these sediments were likely to contain more benthic and settled diatom frustules. As such the decrease in coastal diatom blooms and D*Si* and their offshore transport after the AHD, significantly reduced the supply and accumulation of B*Si* in these stations. Conversely, stations TA05 and G05 that were far removed from this longshore transport from the Nile were little affected by these flood plumes prior to the AHD and lateral sediment transport, and therefore also by their cessation thereafter. The higher B*Si* concentrations at the lower part of cores H04 and H05 relatively to TA05 and G05 sediment cores, may attest to the combined role of the past Nile plume and lateral transport mechanism of sediment and diatom frustules at the relatively narrow shelf and canyons riddled slope near Rosh-Carmel (Jaijel et al., 2023).

3.3. Changes in biogenic silica accumulation rates

Previous ^{14}C dating of pelagic foraminifera from the areas adjacent to cores TA05, H04, H05, and G05 yielded representative mean sedimentation rates (ω) of ~0.012, ~0.03, ~0.016 and ~ 0.005 cm y^{-1}, correspondingly (Hamann et al., 2008; Katz et al., 2020; Zirks et al., 2021). In marine regions with such low sedimentation rates, the activity of unsupported (excess) ^{210}Pb is not considered suitable for dating sediment cores. This is because in such areas, excess ^{210}Pb with its short half-life (22.3 y) is constrained to the mixed layer where its distribution profile is governed by bioturbation rather than decay (Basso et al., 2004). It is however often used for both estimating biological mixing depths (L_b) and calculating mixing coefficients (D_b) in the deep-sea (Basso et al., 2004; Díaz-Asencio et al., 2020). This data was obtained from cores TA05, H04 and G05, where ^{210}Pb activity decreased from the surface downwards (Fig. 6), but not from core H05 where anomalous results disqualified it for our calculations. Biological mixing depths (L_b) in TA05, H04, G05 (seafloor depths 1500, 1100 and 1900 m, respectively) were determined from the estimated depth in the cores where the ^{210}Pb concentrations stabilized (expectedly, where the excess ^{210}Pb is depleted) to be 6, 9 and 3 cm, respectively (Fig. 4). This is in perfect agreement with respective maximal depths of 6 and 9 cm where infauna was found in areas adjacent to the TA05 and H04 stations (H. Lubinevsky, personal communication). Mixing rates in TA05, H04 and G05 were calculated from the ^{14}C sedimentation rates (see above) and the excess ^{210}Pb profiles in the cores to be 0.032, 0.25 and 0.023 $cm^2\ y^{-1}$, respectively, using the least square fit method (e.g. Stordal et al., 1985; Basso et al., 2004). Notably, mixing intensity through the L_b decreases steeply (often exponentially) with depth (Olsen et al., 1981), such that biological mixing processes are much faster near the surface. Calculated transit time beyond the mixed layer (L_b/ω) in the TA05, H04, and G05 cores were 420, 300 and 600 y, delimiting the BSi shift in H04 to <300 y, which supports the AHD impact. The ^{210}Pb fluxes to the seafloor at TA05, H04, and G05 were calculated as $^{210}Pb_{ex}$ inventory x λ to be ~15, ~46 and ~ 5 mBq $cm^{-2}\ y^{-1}$, respectively, where: λ is the decay constant of ^{210}Pb (0.031 y^{-1}) and $^{210}Pb_{ex}$ inventory is the summed multiplications of ^{210}Pb activity (mbq g^{-1}) by the dry sediment weight (g m^{-2}) in the mixed layer (between the surface and the $^{210}Pb_{ex}$ depletion depth).

Previous models and observations demonstrated that over time,

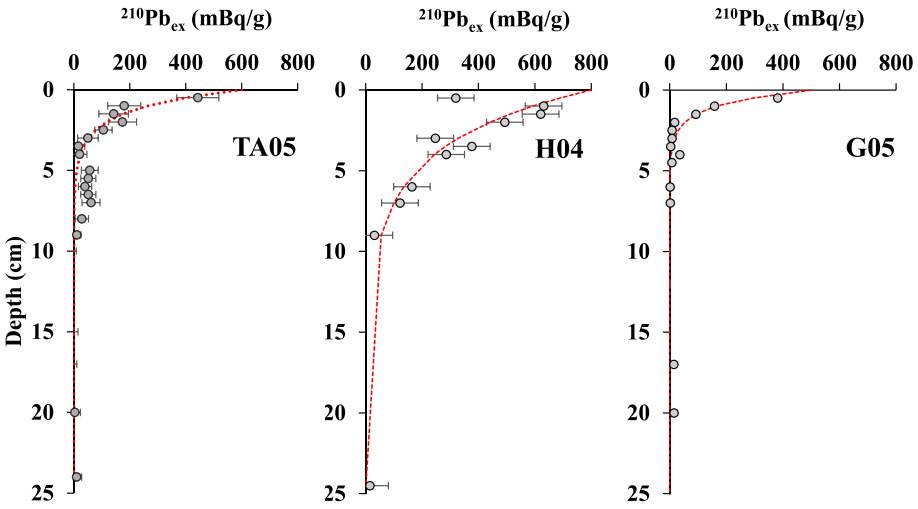

Fig. 6. Estimated excess ^{210}Pb (values above the stable ^{210}Pb disintegrations per gram values at depth) in the cores from TA05, H04 and G05 marked by gray circles. The red dashed lines are from the best fit equations (Stordal et al., 1985) through the measured points down the cores.

temporary decreases in tracer fluxes to the seafloor would manifest in the formation of a subsurface minimum (Steiner et al., 2016). The absence of such a feature in the B*Si* depleted layer in H04 and H05 suggests that the conditions that govern lower preservation of B*Si* in these stations continue. Considering the low sedimentation rates in cores H05 and H04 during the ~55 years since the AHD completion (<3 cm), the respective 5–5.5 cm thickness of the B*Si*-depleted surface layer must be controlled by bioturbation rather than sedimentation.

Based on down core porosities (Fig. 4 and Katz et al., 2020) and assuming a dry sediment density of 2.65 g ml^{-1}, the mean sedimentation rates in the cores were converted to corresponding, mean accumulation rates of ~90, ~183, ~106 and 37 g sediment m^{-2} y^{-1}. Using these rates and BSi concentrations between 6 and 20 cm depth (underneath the BSi depleted surface layer in cores H04 and H05; Fig. 5), we calculated mean accumulation rates of B*Si* in cores TA05, H04, H05, and G05 of 0.2, 0.61, 0.32 and 0.09 g m^{-2} y^{-1}, respectively. Because of its low sedimentation rate (0.005 cm y^{-1}), the 20 cm long G05 core represents the longest sedimentary record indicating that the very low accumulation rates of B*Si* exemplified in this core persisted in the ELB at least during the last ~4000 years.

Assuming that the upper 5 cm in H04 and H05 cores are dominated by mixing and that the overall accumulation rates did not change much, we calculated that the mean burial flux in the upper, 5.5 and 5 cm thick surface layer was only 0.13 and 0.11 g B*Si* m^{-2} y^{-1}, respectively (Supplementary Material). These accumulation rates of B*Si* correspond to only ~21 % and 35 % of the older, pre-shift burial rates and are much closer to these calculated for the far removed TA05 and G05 cores, where B*Si* concentrations did not change.

3.4. Conclusions

This study depicts the ultra-oligotrophic ELB as a unique oceanic setting with extremely low D*Si* concentrations in surface water and B*Si* accumulation rates at the seafloor and demonstrates the dramatic and far reaching (~1000 km south of the study area) effects of the AHD operation since 1965 therein. The ~90 % reduction in the Nile silica discharge by the AHD (Nixon, 2003) caused a decrease in the concentrations and availability of D*Si* to diatoms all along the northern trajectory of the Nile flood plumes, offshore the Israeli Mediterranean coast. Moreover, the mitigation of the Nile summer floods behind the dam, terminated the seasonality of D*Si* and the summer bloom of diatoms in the ELB, setting a new steady state with D*Si* concentration as low as 400 nmol kg^{-1} in the mixed surface layer of this basin. Examination of sediment cores from the slope-base and deep-sea, ~400 km from the Nile outlet, show a dramatic (65–79 %) decrease in B*Si* accumulation rates compared to the pre-AHD rates. These changes were only found in cores along the offshore path of both, the past Nile-plume trajectory and lateral shelf-derived particulate transport while not in remote areas unaffected by these offshore intrusions. These findings demonstrate the far field and ongoing effects of damming on marine ecosystems. Notably, the conditions for diatom growth in the ELB are expected to further deteriorate by ongoing warming combined with reduced rainfall and riverine discharge; all of which increases water column stratification, surface water temperature increases and oligotrophication. In addition to its regional importance, we believe that this research addresses global concerns about the mesoscale mechanisms and extent of which river damming affects the marine ecosystem and the marine silica cycle, particularly in oligotrophic seas.

Credit authorship contribution statement

Timor Katz: Conceptualization, Investigation, Resources, Visualization, Writing – original draft, Writing – review & editing. **Revital Bookman:** Investigation, Resources, Writing – review & editing. **Barak Herut:** Conceptualization, Funding acquisition, Investigation, Resources, Visualization, Writing – original draft, Writing – review & editing. **Beverly Goodman-Tchernov:** Investigation, Writing – review & editing. **Guy Sisma-Ventura:** Conceptualization, Investigation, Resources, Visualization, Writing – original draft, Writing – review & editing.

Declaration of competing interest

The authors declare that they have no known competing financial interests or personal relationships that could have appeared to influence the work reported in this paper.

Data availability

Data will be made available on request.

Acknowledgements

We wish to thank the IOLR Marine Chemistry Department for their help in sampling, analysis and activity in the National Monitoring Program of Israel's Mediterranean waters, supported by the Israeli Ministries of Environmental Protection and Energy. We also thank the crew of the R.V. Bat Galim. We thank Nimer Taha for his assistance in the ^{210}Pb

measurements in the cores.

Appendix A. Supplementary data

Supplementary data to this article can be found online at https://doi.org/10.1016/j.scitotenv.2024.171274.

References

Alkalay, R., Zlatkin, O., Katz, T., Herut, B., Halicz, L., Berman-Frank, I., Weinstein, Y., 2020. Carbon export and drivers in the southeastern Levantine Basin. Deep. Res. Part II 171, 104713. https://doi.org/10.1016/j.dsr2.2019.104713.

Azov, Y., 1991. Eastern Mediterranean-a marine desert? Mar. Pollut. Bull. 23, 225–232. https://doi.org/10.1016/0025-326X(91)90679-M.

Basso, D., Thomson, J., Corselli, C., 2004. Indications of low macrobenthic activity in the deep sediments of the eastern Mediterranean Sea. Sci. Mar. 68, 53–62.

Bernard, C.Y., Laruelle, G.G., Slomp, C.P., Heinze, C., 2010. Impact of changes in river fluxes of silica on the global marine silicon cycle: a model comparison. Biogeosciences 7, 441–453.

Bernard, C.Y., Durr, H.H., Heinze, C., Segschneider, J., Meier-Reimer, E., 2011. Contribution of riverine nutrients to the silicon biogeochemistry in the global ocean—a model study. Biogeosciences 8, 551–564.

Bialik, O.M., Sisma-Ventura, G., 2016. Proxy-based reconstruction of surface water acidification and carbonate saturation of the Levant Sea during the Anthropocene. Anthropocene 16, 42–53.

Browning, T.J., Moore, C.M., 2023. Global analysis of ocean phytoplankton nutrient limitation reveals high prevalence of co-limitation. Nat. Commun. 14, 5014. https://doi.org/10.1038/s41467-023-40774-0.

Brzezinski, M.A., Krause, J.W., Church, M.J., Karl, D.M., Li, B., Jones, J.L., Updyke, B., 2011. The annual silica cycle of the North Pacific subtropical gyre. Deep-Sea Res. I 58, 988–1001.

Chen, Z., Xu, H., Wang, Y., 2021. Ecological degradation of the Yangtze and Nile delta-estuaries in response to dam construction with special reference to monsoonal and arid climate settings. Water (Switzerland) 13, 1–10.

Conley, D.J., 1997. Riverine contribution of biogenic silica to the oceanic silica budget. Limnol. Oceanogr. 42, 774–777.

Conley, D.J., Schelske, C.L., 2001. Biogenic silica. In: Tracking Environmental Changes in Lake Sediments; Terrestrial, Algal, and Siliceous Indicators, 3. Kluwer, pp. 281–293.

Conley, D.J., Stålnacke, P., Pitkänen, H., Wilander, A., 2000. The transport and retention of dissolved silicate from rivers in Sweden and Finland. Limnol. Oceanogr. 45, 1850–1853.

Díaz-Asencio, M., Herguera, J.C., Schwing, P.T., Larson, R.A., Brooks, G.R., Southon, J., Rafter, P., 2020. Sediment accumulation rates and vertical mixing of deep-sea sediments derived from14C and 210Pb in the southern Gulf of Mexico. Mar. Geol. 429, 106288 https://doi.org/10.1016/j.margeo.2020.106288.

Dixit, S., Van Cappellen, P., 2003. Predicting benthic fluxes of silicic acid from deep-sea sediments. J. Geophys. Res. 108 https://doi.org/10.1029/2002JC001309.

Dowidar, N.M., 1984. Phytoplankton biomass and primary productivity of the south-eastern Mediterranean. Deep Sea Res. Part A, Oceanogr. Res. Pap. 31, 983–1000.

Efrati, S., Lehahn, Y., Rahav, E., Kress, N., Herut, B., Gertman, I., Goldman, R., Ozer, T., Lazar, M., Heifetz, E., 2013. Intrusion of coastal waters into the pelagic eastern Mediterranean: in situ and satellite-based characterization. Biogeosciences 10, 3349–3357.

Emery, K., Neev, D., 1960. Mediterranean beaches of Israel. Geol. Surv. Isr. Bull. 26, 1–23.

Gaudette, H.E., Flight, W.R., Toner, L., Folger, D.W., 1974. An inexpensive titration method for the determination of organic carbon in recent sediments. J. Sediment. Res. 44, 249–253.

Halim, Y., 1960. Observations on the nile bloom of phytoplankton in the Mediterranean. ICES J. Mar. Sci. 26, 57–67.

Halim, Y., 1991. The impact of human alterations of the hydrological cycle on ocean margins. In: Mantoura, R.F.A., Martin, J.-M., Wollast, R. (Eds.), Ocean margin processes in Global Change, Dahlem Conferenzen. John Wiley & Sons Ltd., Chichester, pp. 281–300.

Halim, Y., Guergues, S.K., Saleh, H., 1967. Hydrographic conditions and plankton in the South East Mediterranean during the last normal Nile flood (1964). Int. Rev. Hydrobiol. 52, 401–425.

Hamann, Y., Ehrmann, W., Schmiedl, G., Krüger, S., Stuut, J.B., Kuhnt, T., 2008. Sedimentation processes in the Eastern Mediterranean Sea during the Late Glacial and Holocene revealed by end-member modelling of the terrigenous fraction in marine sediments. Mar. Geol. 248, 97–114.

Hecht, A., 1964. On the turbulent diffusion of the water of the Nile floodsin the Mediterranean Sea. Bull. Sea Fish. Res. Stn. Haifa 36, 24 pp.

Herut, B., Almogi-Labin, A., Jannink, N., Gertman, I., 2000. The seasonal dynamics of nutrient and chlorophyll a concentrations on the SE Mediterranean shelf-slope. Oceanol. Acta 23, 771–782.

Herut, B., Guy-Haim, T., Almogi-Labin, A., Hemut, W.F., Ransby, D., Sandler, A., Katz, T., Avnaim-Katav, S., 2023. Marine oligotrophication by starvation of fine sediments and nutrients via anthropogenic sediment and water retention in large rivers, the Nile damming case. Front. Mar. Sci. 10 (2023) https://doi.org/10.3389/fmars.2023.1226379.

Humborg, C., Ittekkot, V., Cociasu, A., von Bodungen, B., 1997. Effect of Danube river dam on Black Sea biogeochemistry and ecosystem structure. Nature 386, 385–388.

Humborg, C., Pastuszak, M., Aigars, J., Siegmund, H., Mörth, C.-M., Ittekkot, V., 2006. Decreased silica land–sea fluxes through damming in the Baltic Sea catchment – significance of particle trapping and hydrological alterations. Biogeochemistry 77, 265–281. https://doi.org/10.1007/s10533-005-1533-3.

Humborg, C., Smedberg, E., Medina, M.R., Mɣrth, C.-M., 2008. Changes in dissolved silicate loads to the Baltic Sea — the effects of lakes and reservoirs. J. Mar. Syst. 73, 223.

Inman, D., Jenkins, S., 1984. The Nile littoral cell and man's impact on the coastal zone of the southeastern Mediterranean. Coast. Eng. Proc. 1, 1600–1617. https://doi.org/10.9753/icce.v19.

Inman, D.L., 2003. Littoral cells. In: Schwartz, M. (Ed.), Encyclopedia of Coastal Science. Kluwer Academic Publishers, Dordrecht, Netherlands, The Earth Sciences Encyclopedia Online, p. 19.

Ittekkot, V., Humborg, C., Schafer, P., 2000. Hydrological alterations and marine biogeochemistry: a silicate issue? Bioscience 50, 776–782.

Jaijel, R., Goodman Tchernov, B.N., Biton, E., Weinstein, Y., Katz, T., 2021. Optimizing a standard preparation procedure for grain size analysis of marine sediments by laser diffraction (MS-PT4SD: marine sediments-pretreatment for size distribution). Deep. Res. Part I Oceanogr. Res. Pap. 167, 103429 https://doi.org/10.1016/j.dsr.2020.103429.

Jaijel, R., Biton, E., Weinstein, Y., Ozer, T., Katz, T., 2023. Observations of turbidity currents in a small, slope-confined submarine canyon in the Eastern Mediterranean Sea. Earth Planet. Sci. Lett. 604, 118008. doi:https://doi.org/10.1016/j.epsl.2023.118008.

Kamykowski, D., Zentara, S.-J., Morrison, J.M., Switzer, A.C., 2002. Dynamic global patterns of nitrate, phosphate, silicate, and iron availability and phytoplankton community composition from remote sensing data. Glob. Biogeochem. Cycles 16 (4), 1077. https://doi.org/10.1029/2001GB001640.

Katz, T., Weinstein, Y., Alkalay, R., Biton, E., Toledo, Y., Lazar, A., Zlatkin, O., Soffer, R., Rahav, E., Sisma-ventura, G., Bar, T., Ozer, T., Gildor, H., Almogi-labin, A., Kanari, M., Berman-frank, I., Herut, B., 2020. The first deep-sea mooring station in the eastern Levantine basin (DeepLev), outline and insights into regional sedimentological processes. Deep. Res. Part II 171, 104663.

Kress, N., Herut, B., 2001. Spatial and seasonal evolution of dissolved oxygen and nutrients in the Southern Levantine Basin (Eastern Mediterranean Sea): chemical characterization of the water masses and inferences on the N:P ratios. Deep Sea Res. Part I Oceanogr. Res. Pap. 48, 2347–2372.

Kress, N., Gertman, I., Herut, B., 2014. Temporal evolution of physical and chemical characteristics of the water column in the Easternmost Levantine basin (Eastern Mediterranean Sea) from 2002 to 2010. J. Mar. Syst. 135, 6–13.

Krom, M.D., Herut, B., Mantoura, F., 2004. Nutrient budget for the Eastern Mediterranean: implications for P limitation. Limnol. Oceanogr. 49, 1582–1592.

Krom, M.D., Kress, N., Fanning, K., 2014. Silica cycling in the ultra-oligotrophic eastern Mediterranean Sea. Biogeosciences 11 (15), 4211–4223.

Laruelle, G.G., Roubeix, V., Sferratore, A., Brodherr, B., Ciuffa, D., et al., 2009. Anthopogenic perturbations of the silicon cycle at the global scale: key role of the land-ocean transition. Glob. Biogeochem. Cycles 23, GB4031.

Leblanc, K., Leynaert, A., Fernandez, I.C., Rimmelin, P., Moutin, T., Raimbault, P., Ras, J., Quéguiner, B., 2005. A seasonal study of diatom dynamics in the North Atlantic during the POMME experiment (2001): evidence for Si limitation of the spring bloom. J. Geophys. Res. Ocean. 110, 1–16. https://doi.org/10.1029/2004JC002621.

Leynaert, A., Treguer, P., Lancelot, C., Rodier, M., 2001. Silicon limitation of the biogenic silica production in the equatorial Pacific. Deep-Sea Res. I 48, 639–660.

Leynaert, A., Bucciarelli, E., Claquin, P., Dugdale, R.C., Martin-Jezequel, V., et al., 2004. Effect of iron deficiency on diatom cell size and silicic acid uptake kinetics. Limnol. Oceanogr. 49, 1134–1143.

Li, M., Wang, H., Li, Y., Ai, W., Hou, L., Chen, Z., 2016. Sedimentary BSi and TOC quantifies the degradation of the Changjiang Estuary, China, from river basin alteration and warming SST. Estuar. Coast. Shelf Sci. 183, 392–401.

Ludwig, W., Dumont, E., Meybeck, M., Heussner, S., 2009. River discharges of water and nutrients to the Mediterranean and Black Sea: major drivers for ecosystem changes during past and future decades? Prog. Oceanogr. 80, 199–217.

Malanotte-Rizzoli, P., Artale, V., Borzelli-Eusebi, G.L., Brenner, S., Crise, A., Gacic, M., Triantafyllou, G., 2014. Physical forcing and physical/biochemical variability of the Mediterranean Sea: a review of unresolved issues and directions for future research. Ocean Sci. 10 (3), 281–322.

Milliman, J.D., 1997. Blessed dams or dammed dams? Nature 386, 325–327.

Mortlock, R.A., Froelich, P.N., 1989. A simple method for the rapid-determination of biogenic opal in pelagic marine-sediments. Deep. Res. Part A-Oceanographic Res. Pap. 36, 1415–1426.

Nixon, S.W., 2003. Replacing the Nile are anthropogenic nutrients providing the fertility once brought to the Mediterranean by a great river? Ambio 32, 30–39.

Noller, J.S., 2000. Lead-210 geochronology. In: Noller, J.S., Sowers, J.M., R., Lettis W. (Eds.), Quaternary Geochronology: Methods and Applications. American Geophysical Union, Washington, D. C, pp. 115–120. https://doi.org/10.1029/RF004p0115.

Olsen, C.R., Simpson, H.J., Peng, T.-H., Bopp, R.F., Trier, R.M., 1981. Lamjnat. J. Geophys. Res. 86, 11020–11028.

Oren, O., Komarovsky, B., 1960. The influence of the Nile flood on the shore waters of Israel. CIESM Conf. 16, 655–659.

Ozer, T., Gertman, I., Kress, N., Silverman, J., Herut, B., 2017. Interannual thermohaline (1979–2014) and nutrient (2002–2014) dynamics in the Levantine surface and intermediate water masses, SE Mediterranean Sea. Glob. Planet. Chang. 151, 60–67.

Ozer, T., Gertman, I., Gildor, H., Herut, B., 2022. Thermohaline temporal variability of the SE Mediterranean coastal waters (Israel) – long-term trends, seasonality, and connectivity. Front. Mar. Sci. 8, 1–14. https://doi.org/10.3389/fmars.2021.799457.
Papush, L., Danielsson, A., 2006. Silicon in the marine environments: dissolved silica trends in the Baltic Sea. Estuar. Coast. Shelf Sci. 67, 53–66.
Pinardi, N., Masetti, E., 2000. Variability of the large-scale general circulation of the Mediterranean Sea from observations and modelling: a review. Palaeogeogr. Palaeoclimatol. Palaeoecol. 158, 153–173.
Pondaven, P., Ragueneau, O., Treguer, P., Hauvespre, A., Dezileau, L., Reyss, J.L., 2000. Resolving the "opal paradox" in the Southern Ocean. Nature 405, 168–172.
Ragueneau, O., Treguer, P., Anderson, R.F., Brzezinski, M.A., DeMaster, D.J., et al., 2000. A review of the Si cycle in the modern ocean: recent progress and missing gaps in the application of biogenic opal as a paleo proxy. Glob. Planet. Chang. 543, 315–366.
Ragueneau, O., Gallinari, M., Corrin, L., Grandel, S., Hall, P., Hauvespre, A., Lampitt, R., Rickert, D., Stahl, H., Tengberg, A., Witbaard, R., 2001. The benthic silica cycle in the Northeast Atlantic: annual mass balance, seasonality, and importance of non-steady-state processes for the early diagenesis of biogenic opal in deep-sea sediments. Prog. Oceanogr. 50, 171–200.
Ragueneau, O., Schultes, S., Bidle, K., Claquin, P., Moriceau, B., 2006. Si and C interactions in the world ocean: importance of ecological processes and implications for the role of diatoms in the biological pump. Glob. Biogeochem. Cycles 20, GB4S02.
Rahav, E., Berman-Frank, I., 2023. Temporal and vertical dynamics of diatoms and dinoflagellates in the southeastern Mediterranean Sea. J. Plankton Res. 1–11.
Rahav, E., Raveh, O., Hazan, O., Gordon, N., Kress, N., Silverman, J., Herut, B., 2018. Impact of nutrient enrichment on productivity of coastal water along the SE Mediterranean shore of Israel - a bioassay approach. Mar. Pollut. Bull. 127, 559–567.
Rahav, E., Silverman, J., Raveh, O., Hazan, O., Rubin-Blum, M., Zeri, C., Gogou, A., Kralj, M., Pavlidou, A., Kress, N., 2019. The deep water of Eastern Mediterranean Sea is a hotspot for bacterial activity. Deep. Res. Part II Top. Stud. Oceanogr. 164, 135–143.
Reich, T., Ben-Ezra, T., Belkin, N., Tsemel, A., Aharonovich, D., Roth-Rosenberg, D., Givati, S., Bialik, M., Herut, B., Berman-Frank, I., Frada, M., Krom, M.D., Lehahn, Y., Rahav, E., Sher, D., 2022. A year in the life of the Eastern Mediterranean: monthly dynamics of phytoplankton and bacterioplankton in an ultra-oligotrophic sea. Deep. Res. Part I Oceanogr. Res. Pap. 182, 103720 https://doi.org/10.1016/j.dsr.2022.103720.
Sayles, F.L., Deuser, W.G., Goudreau, J.E., Dickinson, W.H., Jickells, T.D., King, P., 1996. The benthic cycle of biogenic opal at the Bermuda Atlantic time series site. Deep. Res. Part I Oceanogr. Res. Pap. 43, 383–409. https://doi.org/10.1016/0967-0637(96)00027-1.
Sisma-Ventura, G., Yam, R., Shemesh, A., 2014. Recent unprecedented warming and oligotrophy of the eastern Mediterranean Sea within the last millennium. Geophys. Res. Lett. 41, 5158–5166. https://doi.org/10.1002/2014GL060393.
Sisma-Ventura, G., Kress, N., Silverman, J., Gertner, Y., Ozer, T., Biton, E., Lazar, A., Gertman, I., Rahav, E., Herut, B., 2021. Post-eastern Mediterranean transient oxygen decline in the deep waters of the Southeast Mediterranean Sea supports weakening of ventilation rates. Front. Mar. Sci. 7, 1–10. https://doi.org/10.3389/fmars.2020.598686.
Smetacek, V., 1999. Diatoms and the ocean carbon cycle. Protist 150, 25–32.
Steiner, Z., Lazar, B., Levi, S., Tsroya, S., Pelled, O., Bookman, R., Erez, J., 2016. The effect of bioturbation in pelagic sediments: lessons from radioactive tracers and planktonic foraminifera in the Gulf of Aqaba. Red Sea. Geochim. Cosmochim. Acta 194, 139–152.
Stordal, M.C., Johnson, J.W., Guinasso, N.L., Schink, D.R., 1985. Quantitative evaluation of bioturbation rates in deepp ocean sediments. II. Composition of rates determined by 210Pb, 239,240Pu. Mar. Chem. 17, 99–114.
Tréguer, J.P., De La Rocha, L.C., 2013. The world ocean silica cycle. Annu. Rev. Mar. Sci. 5, 477–501.
Tréguer, P., Nelson, D.M., van Bennekom, A.J., DeMaster, D.J., Leynaert, A., Queguiner, B., 1995. The balance of silica in the world ocean: a re-estimate. Science 268, 375–379.
Turley, C.M., 1999. The changing Mediterranean Sea – a sensitive ecosystem? Prog. Oceanogr. 44, 387–400.
Van Cappellen, P., Qiu, L., 1997. Biogenic silica dissolution in sediments of the Southern Ocean. II. Kinetics. Deep Sea Res. Part II Top. Stud. Oceanogr. 44, 1129–1149. https://doi.org/10.1016/S0967-0645(96)00112-9.
Whaby, S.D., Bishara, N.F., 1980. The effect of the River Nile on Mediterranean water, before and after the construction of the High Dam at Aswan. In: Martin, J.M., Burton, J.D., Eisma, D. (Eds.), River Inputs to Ocean Systems. United Nations, New York, pp. 311–318.
Wollast, R., 1974. The silica problem. In: Sea, The (Ed.), ED Goldberg, 5:365–81. Wiley-Interscience, New York.
Xu, H., Jiang, S., Li, J., Pu, R., Wang, J., Jin, W., Sha, L., Li, D., 2020. Biogenic silica and organic carbon records in Zhoushan coastal sea over the past one hundred years and their environmental indications. Int. J. Environ. Res. Public Health 17, 1–14. https://doi.org/10.3390/ijerph17113890.
Yool, A., Tyrrell, T., 2003. The role of diatoms in regulating the ocean's silicate cycle. Glob. Biogeochem. Cycles 17, 1–24.
Zirks, E., Krom, M., Schmiedl, G., Katz, T., Xiong, Y., Alcott, L.J., Poulton, S.W., Goodman-Tchernov, B., 2021. Redox evolution and the development of oxygen minimum zones in the Eastern Mediterranean Levantine basin during the early Holocene. Geochim. Cosmochim. Acta 297, 82–100.